JOURNAL OF AIRCRAFT
Vol. 33, No. 4, July–August 1996

Multipoint Inverse Airfoil Design Method for Slot-Suction Airfoils

Farooq Saeed* and Michael S. Selig†
University of Illinois at Urbana–Champaign, Urbana, Illinois 61801

Owing to a renewed interest in advanced-concept transport aircraft with active boundary-layer control (suction and/or blowing), a generalized multipoint method for the inverse design of airfoils with slot suction in incompressible potential flow is presented. The results predicted by theory show good agreement with experiment. Such a design tool could be used interactively to perform rapid trade studies to examine the potential payoff for boundary-layer control as applied to the advanced-concept wings. The method, which is based on conformal mapping, draws on the theory first published by Eppler (*Airfoil Design and Data*, Springer–Verlag, New York, 1990) and extended by Selig and Maughmer ("A Multipoint Inverse Airfoil Design Method Based on Conformal Mapping," *AIAA Journal*, Vol. 30, No. 5, 1992, pp. 1162–1170). The theory predicts an increased lift coefficient and a nonzero value for the inviscid drag coefficient as a result of the slot suction, a price to be paid for the increased lift. The theory also shows that this nonzero value of the inviscid drag coefficient is exactly equal to twice the suction coefficient. Two examples are discussed to illustrate the method and the corresponding change in the aerodynamic characteristics of the airfoils as a result of slot suction.

Nomenclature

a_m, b_m = Fourier series coefficients
b = location of the suction slot, $\zeta = e^{i\beta}$
C_d = airfoil drag coefficient
C_l = airfoil lift coefficient
C_Q = suction coefficient
c = airfoil chord
D = airfoil drag
d = location of the stagnation point downstream of the suction slot, $\zeta = e^{i\delta}$
F_x, F_y = x and y components of force
$F(z)$, $F(\zeta)$ = complex potential functions
f = front stagnation point, $\zeta = e^{i\gamma}$
$g(\phi)$, $h(\phi)$ = positive, nonzero functions
K, $\bar{K}$ = main recovery parameters
K_H, $\bar{K}_H$ = closure recovery parameters
L = airfoil lift
M_0 = airfoil pitching moment
$P(\phi)$, $Q(\phi)$ = harmonic functions on unit circle
Q_s = suction strength
$Q_s^*(\phi)$ = multipoint design suction strength distribution
t/c = airfoil thickness-to-chord ratio
V_∞ = freestream velocity
v_i = design velocity level for segment i
$\tilde{v}_i(\tilde{\phi}_i)$ = relative design velocity distribution for segment i
$v^*(\phi)$ = multipoint design velocity distribution
$w(\phi)$ = total recovery function
$w_D(\phi, i)$ = suction distribution function
$w_Q(\phi, i)$ = main suction function for segment i
$x(\phi)$, $y(\phi)$ = airfoil coordinates
z = airfoil–plane complex coordinate, $x + iy$
α = angle of attack from zero-lift angle
α_i = angle of attack from zero-lift angle for segment i
α_{0L} = angle of attack for zero lift
$\alpha^*(\phi)$ = multipoint design angle-of-attack distribution
β_i = design location of the suction slot for segment i
$\beta^*(\phi)$ = multipoint design suction-slot location distribution
Γ = circulation strength
$\gamma^*(\phi)$ = multipoint design front stagnation point distribution
δ_i = design location of the stagnation point downstream of the suction slot for segment i
$\delta^*(\phi)$ = multipoint design slot-suction stagnation point distribution
ε = trailing-edge angle parameter
ζ = circle–plane complex coordinate, $\xi + i\eta$ or $e^{i\phi}$
$\theta^*(\phi)$ = design distribution of the flow direction about airfoil
μ, $\bar{\mu}$ = main recovery parameters
$\pi^*(\phi)$ = step function
ρ = fluid density
ϕ_i = arc limit for segment denoting junction between segments i and $i + 1$
$\tilde{\phi}_i$ = relative arc limit for segment i, $\phi - \phi_{i-1}$
ϕ_S, $\tilde{\phi}_S$ = closure recovery arc limits

Subscripts
$+$ = approach from positive side
$-$ = approach from negative side

Received May 13, 1995; presented as Paper 95-1857 at the AIAA 13th Applied Aerodynamics Conference, San Diego, CA, June 19–22, 1995; revision received March 21, 1996; accepted for publication March 26, 1996.

*Graduate Research Assistant, Department of Aeronautical and Astronautical Engineering, 306 Talbot Laboratory, 104 South Wright Street. Student Member AIAA.

†Assistant Professor, Department of Aeronautical and Astronautical Engineering, 306 Talbot Laboratory, 104 South Wright Street. Member AIAA.

Introduction

ALTHOUGH conventional configurations for the subsonic commercial or transport aircraft are most widely accepted, there is growing interest among the aerospace engineering community in some of the advanced concepts such as the Goldschmied's thick-wing spanloader all-freighter[1] shown in Fig. 1. Goldschmied's conceptual design study was based

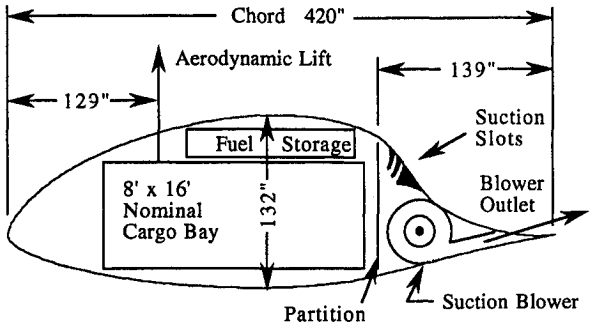

Fig. 1 Layout of the modified GLAS II 31.5%-thick laminar-flow airfoil with a 10.3-m chord (adapted from Ref. 1).

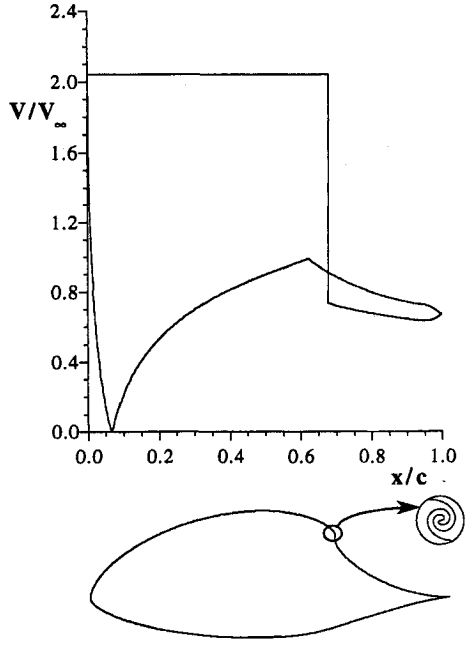

Fig. 2 Velocity distribution of a 35%-thick Glauert-type airfoil.

on a synthesis of proven technologies. Some of these were the 1946 Northrop XB-35 Flying Wing, the 1951 31.5%-thick modified GLAS II laminar-flow airfoil with slot-suction boundary-layer control, and the Goldschmied high-efficiency centrifugal blower. The results of the study revealed that the thick-wing spanloader had an aerodynamic transport efficiency[1] of 25 as compared with a maximum value of 10 for the conventional cargo aircraft. The results were based on the use of suction slots to remove the boundary layer at the points on the airfoil where the flow has a tendency to separate. Thus, very thick airfoils could be designed to exhibit laminar flow characteristics over a greater part of the surface throughout a C_l range that is large enough to completely cover the normal flight range, and which are also thick enough to provide ample room for the stowage of engines, passengers, and other loads. The fact that very large lift coefficients can be obtained from thick airfoils with active boundary-layer control (suction and/or blowing) without separation has not only been predicted through analytical models such as those of Glauert,[2-4] but has also been confirmed through numerous experimental studies.[5-10] Recently, these studies have generated a renewed interest[11-13] in such advanced concepts.

Glauert's method[2-4] for the design of slot-suction airfoils is well known. It is interesting, however, that Glauert's method does not actually account for suction at the slot location. It can be shown that for slot suction on an airfoil, a stagnation point must exist on the airfoil surface just downstream of the slot. Glauert's airfoils do not exhibit this characteristic feature. Moreover, there is no specified parameter related to the amount of suction. Instead, the velocity distributions of Glauert-type airfoils (see Fig. 2) show a step drop in the velocity at the location of the slot. Lighthill[14] has also suggested the same strategy for designing airfoils with slot suction. This type of velocity distribution can be obtained by making the pressure recovery infinitely steep at the slot location. The point of the infinitely steep pressure recovery is represented on the airfoil surface by an infinite spiral (shown in exaggerated view in Figs. 2 and 3). On the surface as the flow enters the spiral, the velocity approaches the value before the drop. On the way out of the spiral (on the other side of the spiral inlet), the velocity is equal to the value past the drop.

Although clear from the theory, it is possible to verify computationally that Glauert's well-known GLAS II airfoil shown in Fig. 3a was designed by prescribing a step drop (step function) in the velocity distribution at the slot location. The panel method of the Eppler code[15,16] was used to produce the velocity distribution shown in Fig. 3a. The resulting velocity distribution exhibits minor oscillations on either side of the step drop similar to the Gibbs phenomenon observed when a step function is approximated by a regular or smooth function. The computer program described in Selig and Maughmer[17] was used to design an airfoil that nearly matched the GLAS II airfoil shape. The airfoil shown in Fig. 3b was designed to have a very steep drop in the velocity distribution at the slot location to simulate a step function. No suction was used in the design. The resulting airfoil is almost identical in every respect to the GLAS II airfoil, which verifies that Glauert's airfoil did not employ suction, but a step drop in the velocity as expected.

A design method for slot-suction airfoils should include the effects of true suction at the slot location; that is, the flow

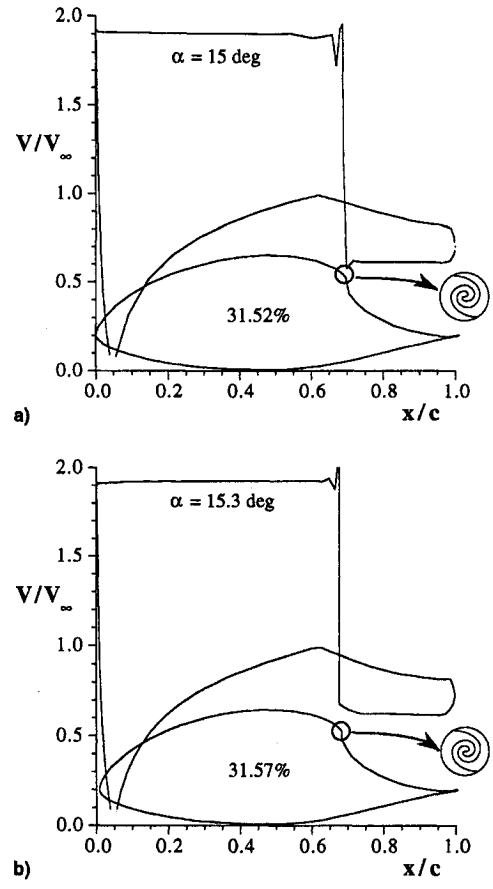

Fig. 3 a) Glauert's well-known GLAS II airfoil analyzed by the panel method of Eppler code[15,16] and b) airfoil designed by the method of Selig and Maughmer[17] using GLAS II's velocity distribution.

model should first include a sink on the airfoil surface at the slot-suction location. Second, since the primary purpose of suction is to improve the airfoil performance by removing the boundary layer, which would otherwise separate owing to a sharp pressure rise in the pressure recovery region, it makes it necessary to integrate the development of the associated viscous boundary layer into the multipoint inverse design method so that it can lead to the design of practical airfoils. With such a design method in hand, several practical issues could be addressed and interesting tradeoffs could be explored. For example, for a desired net pressure recovery, how much suction is required? Alternatively, for a set amount of suction, how much pressure recovery can be achieved? Is it advantageous to vary the amount of suction depending on the flight conditions? Also, how much power is required for the suction system based on mass flow requirements? Although these interesting and important design-related questions are not currently addressed, the inviscid inverse design method presented here could in the future be extended to include viscous effect and thereby pave the way toward furthering our understanding of the myriad of tradeoffs involved in the design of advanced-concept aircraft that take advantage of the slot suction.

Theory

The theory behind the design of airfoils with slot suction is similar to that presented by Selig and Maughmer[17]; the difference derives principally from the presence of a sink on the airfoil surface. Although the presence of the sink in the flow introduces a singularity into the flowfield, it is a good representation or model of the suction effect on the velocity distribution, i.e., the velocity increases in front of the suction slot and decreases behind it.[18] A conceptual illustration of the flow around a circle and an airfoil with slot (point) suction is shown in Fig. 4.

The flow in the ζ plane is modeled by the presence of a uniform flow of unit velocity at an angle of attack α, a vortex of strength Γ at the origin, and a point sink of strength $Q_s (Q_s < 0)$. The sink is placed at $\zeta = b$ in the flowfield so that when a unit circle centered at the origin is added to the flow, using the Milne-Thomson circle theorem,[19] it falls on the boundary of the circle at $\zeta = b = e^{i\beta}$. The complex potential for the flowfield with the circle added is given by

$$F(\zeta) = e^{-i\alpha} + (e^{i\alpha}/\zeta) + (Q_s/2\pi)\ell n(\zeta - b) + (Q_s/2\pi)\ell n[(1/\zeta) - \bar{b}] + i(\Gamma/2\pi)\ell n\,\zeta \tag{1}$$

and where

$$\Gamma = 4\pi \sin\alpha - Q_s \cot(\beta/2) \tag{2}$$

is the circulation strength required to satisfy the Kutta condition by fixing the rear stagnation point at $\zeta = 1$.

Since a stagnation point must exist downstream of the suction slot, say, at $\zeta = d = e^{i\delta}$ on the circle, imposing this condition requires that

$$Q_s = -8\pi \sin(\beta/2)\sin[(\beta - \delta)/2]\cos[\alpha - (\delta/2)] \tag{3}$$

The front stagnation point is then located at $\zeta = f = e^{i\gamma}$, where $\gamma = \pi + 2\alpha + \beta - \delta$. And the complex velocity is given by

$$\frac{dF}{d\zeta} = \left(1 - \frac{1}{\zeta}\right)\left(1 - \frac{d}{\zeta}\right)\left(1 - \frac{b}{\zeta}\right)^{-1}\left(1 - \frac{f}{\zeta}\right)e^{-i\alpha} \tag{4}$$

which on the circle $\zeta = e^{i\phi}$ becomes

$$\left.\frac{dF}{d\zeta}\right|_{\zeta=e^{i\phi}} = 4\sin\left(\frac{\phi}{2}\right)\sin\left(\frac{\phi - \delta}{2}\right)\csc\left(\frac{\phi - \beta}{2}\right) \times \cos\left(\frac{\phi - \beta + \delta}{2} - \alpha\right)e^{-i(\phi - \pi/2)} \tag{5}$$

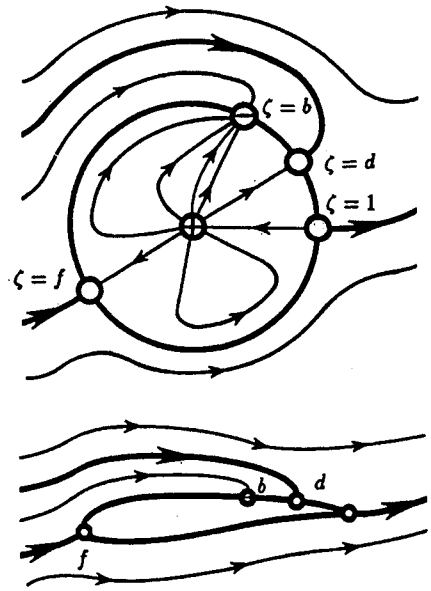

Fig. 4 Conceptual illustration of the flow around a circle and an airfoil with slot suction. The symbol ⊕ indicates a doublet and a source, ⊖ a sink pair, and ○ a stagnation point.

The complex velocity about the circle in the ζ plane is alternatively written as

$$\left.\frac{dF}{d\zeta}\right|_{\zeta=e^{i\phi}} = 4\sin\left(\frac{\phi}{2}\right)\left|\sin\left[\frac{\phi - \delta^*(\phi)}{2}\right]\csc\left[\frac{\phi - \beta^*(\phi)}{2}\right]\right| \times \left|\cos\left[\frac{\phi - \beta^*(\phi) + \delta^*(\phi)}{2} - \alpha^*(\phi)\right]\right| e^{-i[\phi - \pi/2 - \pi^*(\phi)]} \tag{6}$$

where

$$\pi^*(\phi) = \begin{cases} 0, & 0 \le \phi \le \delta^*(\phi) \\ \pi, & \delta^*(\phi) \le \phi \le \beta^*(\phi) \\ 0, & \beta^*(\phi) \le \phi \le \gamma^*(\phi) \\ \pi, & \gamma^*(\phi) \le \phi \le 2\pi \end{cases} \tag{7}$$

is a step function introduced to account for the jumps in the flow direction at the two stagnation points and at the suction slot. The asterisk mark refers to the desired design conditions.

The flow about the circle in the ζ plane is mapped to the flow about an arbitrary airfoil in the z plane via $z = z(\zeta)$ (see Fig. 5). The derivative of the mapping function on the unit circle is assumed to be of the form

$$\left.\frac{dz}{d\zeta}\right|_{\zeta=e^{i\phi}} = (1 - e^{-i\phi})^{1-\varepsilon}\exp\sum_{m=0}^{\infty}(a_m + ib_m)e^{-im\phi} = (1 - e^{-i\phi})^{1-\varepsilon}e^{P(\phi)+iQ(\phi)} \tag{8}$$

which must satisfy three conditions: 1) the airfoil trailing-edge angle must be finite, 2) the flow at infinity must be unaltered, and 3) the airfoil contour must close. These conditions on the mapping lead to the integral constraints[17] that must be satisfied for multipoint inverse airfoil design.

The complex velocity in the z plane on the boundary of the unit circle is expressed as

$$\left.\frac{dF}{dz}\right|_{\zeta=e^{i\phi}} = v(\phi)e^{-i\theta(\phi)} \tag{9}$$

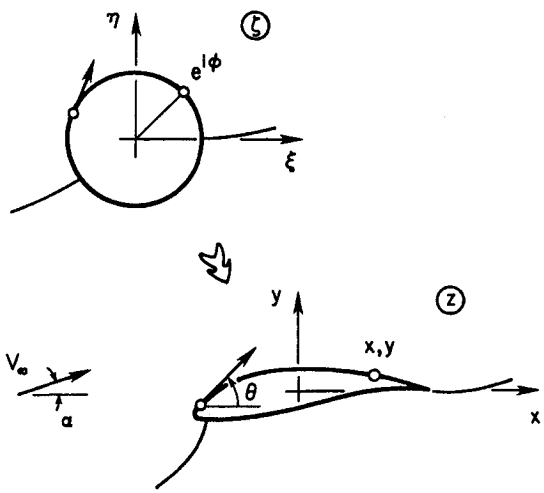

Fig. 5 Mapping from the circle to airfoil plane (slot suction omitted for clarity).

To reflect the jumps in the flow direction, the previous equation is rewritten as

$$\left.\frac{dF}{dz}\right|_{\zeta=e^{i\phi}} = v^*(\phi)e^{-i\theta^*(\phi)} \tag{10}$$

where $|v(\phi)| = v^*(\phi)$ and $\theta(\phi)$ is replaced by $\theta^*(\phi)$. To relate $v^*(\phi)$ and $\theta^*(\phi)$ to the series coefficient of the mapping derivative, the complex velocity is written alternatively as

$$\left.\frac{dF}{dz}\right|_{\zeta=e^{i\phi}} = \frac{\left(\frac{dF}{d\zeta}\right)_{\zeta=e^{i\phi}}}{\left(\frac{dz}{d\zeta}\right)_{\zeta=e^{i\phi}}} \tag{11}$$

Substituting Eqs. (6) and (8) into Eq. (11) and taking the natural logarithm of the resulting equation yields the following result:

$$P(\phi) = -\ell n\left\{\frac{1}{2}\left(2\sin\frac{\phi}{2}\right)^{-\varepsilon}\left|\sin\left[\frac{\phi-\beta^*(\phi)}{2}\right]\right.\right.$$
$$\times \csc\left[\frac{\phi-\delta^*(\phi)}{2}\right]\Bigg| v^*(\phi)$$
$$\left.\left.\times\left|\sec\left[\frac{\phi-\beta^*(\phi)+\delta^*(\phi)}{2}-\alpha^*(\phi)\right]\right|\right\} \tag{12}$$

$$Q(\phi) = \theta^*(\phi) + \pi^*(\phi) - (\phi/2) + \varepsilon[(\pi/2) - (\phi/2)] \tag{13}$$

where $0 \leq \phi \leq 2\pi$.

Thus, the specification of velocity $v^*(\phi)$, the angle of attack $\alpha^*(\phi)$, the location of the suction slot $\beta^*(\phi)$, and the location of the stagnation point downstream of the suction slot $\delta^*(\phi)$ uniquely determines $P(\phi)$. Alternatively, specifying the airfoil flow direction $\theta^*(\phi)$, $\alpha^*(\phi)$, $\beta^*(\phi)$, and $\delta^*(\phi)$ uniquely determines $Q(\phi)$. Since $P(\phi)$ and $Q(\phi)$ are conjugate harmonic functions, then from either one the corresponding harmonic function is determined through the Poisson's integral formula exterior to the circle. Once $P(\phi)$ and $Q(\phi)$ are known, the airfoil coordinates $x(\phi)$ and $y(\phi)$ are then obtained through quadrature.

Multipoint Design Capability of the Theory

The function $P(\phi)$ depends only on ϕ and is defined by specifying $v^*(\phi)$, $\alpha^*(\phi)$, $\beta^*(\phi)$, and $\delta^*(\phi)$, now called the design velocity distribution and the corresponding distributions of the design angle of attack, location of the suction slot, and the stagnation point downstream of the suction slot, respectively. Since it is only necessary that $P(\phi)$ be continuous, a discontinuity in any one or a combination of the design variables, i.e., $v^*(\phi)$, $\alpha^*(\phi)$, $\beta^*(\phi)$, and $\delta^*(\phi)$, must be compensated by a corresponding discontinuity in any one or a combination of the remaining design variables. This is the most important point of the theory, and it is on this basis that the multipoint design is accomplished. Thus, the airfoil can be divided into a number of segments along which the design velocity distribution along with the design values for $\alpha^*(\phi)$, $\beta^*(\phi)$, and $\delta^*(\phi)$ are specified. It is helpful for design purposes to let $\alpha^*(\phi)$, $\beta^*(\phi)$, and $\delta^*(\phi)$ be constant over any given segment; whereas $v^*(\phi)$ should be allowed to vary to obtain some desired velocity distribution. Then, to ensure continuity between segments, the following condition must be satisfied:

$$P_+(\phi_i) = P_-(\phi_i) \tag{14}$$

or from Eq. (12)

$$\left|\frac{v^*_+(\phi_i)\sin\left[\frac{\phi_i-\beta^*_+(\phi_i)}{2}\right]\csc\left[\frac{\phi_i-\delta^*_+(\phi_i)}{2}\right]}{\cos\left[\frac{\phi_i-\beta^*_+(\phi_i)+\delta^*_+(\phi_i)}{2}-\alpha^*_+(\phi_i)\right]}\right|$$
$$= \left|\frac{v^*_-(\phi_i)\sin\left[\frac{\phi_i-\beta^*_-(\phi_i)}{2}\right]\csc\left[\frac{\phi_i-\delta^*_-(\phi_i)}{2}\right]}{\cos\left[\frac{\phi_i-\beta^*_-(\phi_i)+\delta^*_-(\phi_i)}{2}-\alpha^*_-(\phi_i)\right]}\right| \tag{15}$$

where ϕ_i is the arc limit between segments i and $i+1$. Thus, different design parameters [e.g., slot-suction location $\beta^*(\phi)$] or operating conditions may be specified with respect to different segments on the circle yielding a multipoint design.

Airfoil Lift, Drag, and Moment

The forces and the pitching moment acting on the airfoil are determined from the Blasius relations, which are

$$F_x - iF_y = i\frac{\rho}{2}\oint_{C_z}\left(\frac{dF}{dz}\right)^2 dz \tag{16}$$

$$M_0 = \frac{\rho}{2}Re\left[\oint_{C_z}\left(\frac{dF}{dz}\right)^2 z\,dz\right] \tag{17}$$

where C_z is any closed curve that encircles the airfoil. The resulting airfoil lift and drag components of the forces are

$$L = \rho\Gamma \tag{18a}$$

$$D = -\rho Q_s \tag{18b}$$

which in coefficient form are

$$C_l = 2\Gamma/c \tag{19a}$$

$$C_d = -2Q_s/c \tag{19b}$$

Substituting Eqs. (2) and (3) into the previous equation yields

$$C_l = (8\pi/c)\sin\alpha - (2Q_s/c)\cot(\beta/2) \tag{20}$$

$$C_d = (16\pi/c)\sin(\beta/2)\sin[(\beta-\delta)/2]\cos[\alpha-(\delta/2)] \tag{21}$$

It is interesting that the lift–curve slope is still nominally 2π, with suction Q_s providing an offset to the lift coefficient. More-

over, an expression for the angle of attack for zero-lift α_{0L} can be obtained from Eq. (20) by setting C_l equal to zero. It is given by

$$\alpha_{0L} = \sin^{-1}[(Q_s/4\pi)\cot(\beta/2)] \tag{22}$$

It shows that the angle of attack for zero-lift α_{0L} not only depends on the amount of suction Q_s, but also on the location of the suction slot, i.e., β.

If we now define C_Q as

$$C_Q = Q_s/V_\infty c \tag{23}$$

comparing Eq. (19b) and Eq. (23) yields an important result of the analysis that

$$C_d = -2C_Q \tag{24}$$

Note that for $Q_s < 0$, which corresponds to suction, a positive value for the inviscid drag coefficient results. Thus, the introduction of slot suction on the airfoil not only results in an increased lift because of increased circulation around the airfoil, but also in a nonzero value for the inviscid drag, which is purely because of suction. The magnitude of the inviscid drag coefficient is found to be exactly twice that of the slot-suction coefficient. This result that suction produces drag is in contrast to the speculations of Goldschmied[1] that slot suction results in a thrust.

The expression for the pitching moment about the origin of the z plane (positive clockwise) is given by

$$M_0 = 2\pi\rho(b_2\cos 2\alpha - \{a_2 + [(\varepsilon - 1)/2]\}\sin 2\alpha) + 2\rho Q_s \sin(\alpha - \beta) - (\rho\Gamma Q_s/2\pi) \tag{25}$$

where

$$a_2 = \frac{1}{\pi}\int_0^{2\pi} P(\phi)\cos 2\phi \, d\phi \tag{26a}$$

$$b_2 = \frac{1}{\pi}\int_0^{2\pi} P(\phi)\sin 2\phi \, d\phi \tag{26b}$$

Solution Formulation

Like in any inverse design method, the specification of velocity is not completely arbitrary. To satisfy the three integral constraints on $P(\phi)$, the specification of $P(\phi)$ through $v^*(\phi)$, $\alpha^*(\phi)$, $\beta^*(\phi)$, and $\delta^*(\phi)$ must contain at least three free parameters to be determined by solution. Selig and Maughmer[17] introduce these three parameters in a way that facilitates the numerical solution, allows for implementation into a multidimensional Newton iteration, and makes it possible to design practical airfoils. The same approach is used here for the inverse design of airfoils with slot suction.

Velocity Laws

The prescribed velocity distribution must satisfy not only the integral constraints and the continuity conditions, but in the vicinity of the singular points of the flow, it must follow a special law. This condition is apparent from Eq. (12), which gives

$$v^*(\phi) = 2e^{-P(\phi)}\left(2\sin\frac{\phi}{2}\right)^{\varepsilon}\left|\sin\left[\frac{\phi - \delta^*(\phi)}{2}\right]\right| \times \csc\left[\frac{\phi - \beta^*(\phi)}{2}\right]\left|\cos\left[\frac{\phi - \beta^*(\phi) + \delta^*(\phi)}{2} - \alpha^*(\phi)\right]\right| \tag{27}$$

In addition to the leading- and trailing-edge stagnation point velocity laws dictated by the last cosine term and the term $(2\sin\phi/2)^{\varepsilon}$, respectively, the velocity in the vicinity of $\beta^*(\phi)$ must conform to the following laws:

$$\lim_{\phi_+ \to \beta^*(\phi)} v^*(\phi) \sim \left|\csc\left[\frac{\phi - \beta^*(\phi)}{2}\right]\right| g_+(\phi) \tag{28a}$$

$$\lim_{\phi_- \to \beta^*(\phi)} v^*(\phi) \sim \left|\csc\left[\frac{\phi - \beta^*(\phi)}{2}\right]\right| g_-(\phi) \tag{28b}$$

and at $\delta^*(\phi)$ it must follow that

$$\lim_{\phi_+ \to \delta^*(\phi)} v^*(\phi) \sim \left|\sin\left[\frac{\phi - \delta^*(\phi)}{2}\right]\right| h_+(\phi) \tag{29a}$$

$$\lim_{\phi_- \to \delta^*(\phi)} v^*(\phi) \sim \left|\sin\left[\frac{\phi - \delta^*(\phi)}{2}\right]\right| h_-(\phi) \tag{29b}$$

where the functions $g(\phi)$ and $h(\phi)$ are positive nonzero functions.

Specification of the Velocity Distribution

The form used for the specification of the velocity distribution is similar to that given by Selig and Maughmer,[17] except that now we introduce a new function $w_Q(\phi, i)$, called the suction function for segment i, into the velocity distribution so that it conforms to the additional velocity laws given by Eqs. (28) and (29). The new forms for the specification of the design velocity distribution for the recovery and intermediate segments, respectively, are then given by

$$v^*(\phi) = v_i w(\phi) w_Q(\phi, i) \tag{30a}$$

$$v^*(\phi) = [v_i + \tilde{v}_i(\tilde{\phi}_i)]w_Q(\phi, i) \tag{30b}$$

where $\phi_{i-1} \le \phi \le \phi_i$. These are accompanied by the specification of the design values for $\alpha^*(\phi) = \alpha_i$, $\beta^*(\phi) = \beta_i$, and $\delta^*(\phi) = \delta_i$ for that segment. Since it is more convenient (for design purposes) to specify the suction strength distribution $Q_s^*(\phi)$ instead of $\delta^*(\phi)$, the latter is found numerically from Eq. (3) for a given set of design conditions.

Suction Function

With this method, airfoils may be designed with the suction slot present on a segment at its design condition. For such a segment (one designed with slot suction on the segment), now termed an on-suction segment, the velocity distribution must satisfy the velocity laws given by Eqs. (28) and (29). However, on any segment outside of the on-suction segment, now termed as the off-suction segment, it is not necessary for the velocity distribution to conform to the velocity laws. To implement these ideas, the suction function, for the ith segment when suction is present, is given by

$$w_Q(\phi, i) = \left|\frac{\sin[(\phi - \delta_i/2)]}{\sin[(\phi - \beta_i)/2]}\right| w_D(\phi, i) \tag{31}$$

for on-suction segments, i.e., $\phi_{i-1} < \beta_i < \phi_i$, otherwise for off-suction segments it is set equal to 1. The function $w_D(\phi, i)$ is any distribution/interpolating function, which as a matter of convenience satisfies the conditions

$$w_Q(\phi_{i-1}, i) = w_Q(\phi_i, i) = 1 \tag{32}$$

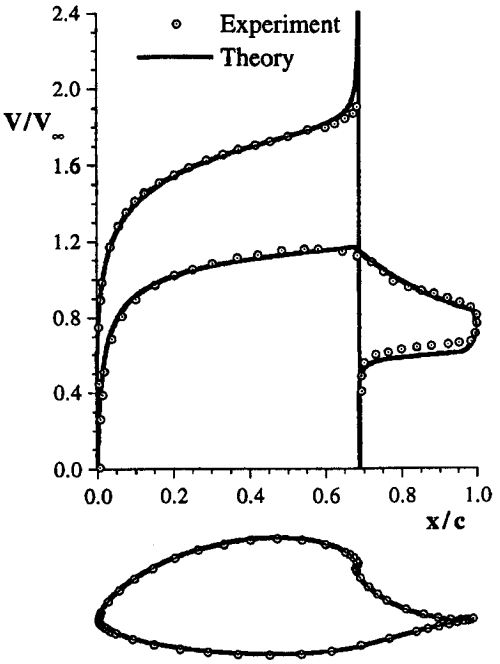

Fig. 6 Comparison of theoretical and experimental results for $C_Q = -0.0106$ and $\alpha = 6$ deg.

A convenient choice for $w_D(\phi, i)$ is that of a linear function given by

$$w_D(\phi, i) = \frac{\left|\sin\left(\frac{\phi_{i-1} - \beta_i}{2}\right)\right|}{\left|\sin\left(\frac{\phi_{i-1} - \delta_i}{2}\right)\right|}\left(\frac{\phi - \phi_i}{\phi_{i-1} - \phi_i}\right) + \frac{\left|\sin\left(\frac{\phi_i - \beta_i}{2}\right)\right|}{\left|\sin\left(\frac{\phi_i - \delta_i}{2}\right)\right|}\left(\frac{\phi - \phi_{i-1}}{\phi_i - \phi_{i-1}}\right) \tag{33}$$

Validation of Theoretical Results

A five-segment airfoil was designed to match the Glauert GLAS II airfoil, which has a suction slot at $0.69c$ and $t/c_{max} = 0.315$. The resulting airfoil shape and velocity distributions are shown in Fig. 6 in comparison with the experiment.[20] Both the experimental and theoretical results correspond to $C_Q = -0.0106$ and $\alpha = 6$ deg and show good agreement. The theoretical results yield a C_l of 0.86 and a C_d of 0.0212 as compared with a C_l of 0.92 and a C_d of 0.004 from experiment. The difference in the values of C_d is because the experimental results were obtained from a wake survey and therefore do not account for the drag component because of suction; whereas, the theoretical results account for inviscid drag caused by suction alone.

Design Examples

Two examples are presented in this section merely to demonstrate the design procedure and to illustrate the capabilities of the method. In the discussion that follows, only those aspects that are unique to the integration of the slot suction into the method are discussed in detail, since the other more general issues can be found in Ref. 17.

As a first example, the design of a five-segment Glauert-type airfoil with a cusped trailing edge $\varepsilon = 0$ is presented. Table 1 lists the initial values of some of the design variables. For simplicity, the design distributions of the suction-slot location and the corresponding suction strength are specified as constants over all segments, i.e., $\beta^*(\phi) = 51.5$ deg and $Q_s^*(\phi) = -0.22$, respectively, which can be different for each segment based on the multipoint design requirements. Moreover, for segment 2, the relative design velocity distribution function $\tilde{v}_2(\tilde{\phi}_2)$ is prescribed as a linear function of $\tilde{\phi}_2$ by the following relation:

$$\tilde{v}_2(\tilde{\phi}_2) = \frac{\tilde{\phi}_2}{(\phi_3 - \phi_2)}\left(\frac{d\tilde{v}_2}{d\tilde{\phi}_2}\right) \tag{34}$$

where the slope $(d\tilde{v}_2/d\tilde{\phi}_2)$, is set equal to 1.3.

Table 1 Initial values of the design variables

i	ϕ_i, deg	α_i, deg	v_i
1	40.00	15.52	$v_1 = 0.63$, $K = 1$, $\phi_S = 18$ deg
2	54.00	15.52	v_2
3	192.58	15.52	v_3
4	290.51	00.22	v_4
5	360.00	00.22	v_5, $\bar{K} = 1$, $\tilde{\phi}_S = 348$ deg

Table 2 Converged solution

i	ϕ_i, deg	α_i, deg	δ_i, deg	v_i	C_l	C_d
1	40.00	15.73	49.16	0.712	2.39	0.136
2	61.42	15.73	49.16	0.712	2.39	0.136
3	194.52	15.73	49.16	2.012	2.39	0.136
4	292.09	00.01	48.96	1.253	0.28	0.136
5	360.00	00.01	48.96	1.253	0.28	0.136

After having defined all of the independent variables in the design, as the next step, the eight unknowns, v_2, v_3, v_4, v_5, μ, $\bar{\mu}$, K_H, and $\bar{K}_H$ are determined. First of all, the continuity condition, Eq. (15), is used to determine the velocity levels v_2, v_3, v_4, and v_5. The values of μ, $\bar{\mu}$, K_H, and $\bar{K}_H$ are then determined from the solution of a system of equations. The complete design velocity distribution $v^*(\phi)$ is then obtained and used to form $P(\phi)$ along with the other design variables. The conjugate harmonic function $Q(\phi)$ is then determined through the Poisson's integral. Finally, the airfoil coordinates are computed from $P(\phi)$ and $Q(\phi)$.

To obtain an airfoil with an uncrossed trailing edge, a trailing-edge velocity ratio of less than unity is required. The trailing-edge velocity ratio of less than unity can usually be obtained when the sum $K_H + \bar{K}_H$ is in the range 0–0.8. Since the initial values for the design may not yield a sum within this range, a multidimensional Newton iteration is employed in the design to accomplish this task. In this process, a desired value for the dependent variable is obtained by iterating on the value of an independent design variable. During each iteration, the process outlined in the previous paragraph is repeated until the calculated values are within a given tolerance of the desired values. This procedure is usually performed in stages.

For example, for the airfoil under discussion, initially a two-dimensional Newton iteration is performed to obtain $K_H = -0.35$ and $\bar{K}_H = 0.30$. This is accomplished by iterating on the leading-edge arc limit ϕ_3 and the velocity level v_1, respectively. After obtaining a converged solution, a third variable is added to the Newton iteration by requiring that $(t/c)_{max} = 0.315$, which is equal to that of the GLAS II airfoil. This desired thickness is achieved by increasing the upper-surface $\alpha^*(\phi)$ by a given amount and decreasing the lower-surface values by the same amount. After obtaining a converged solution, two more variables are introduced into the Newton iteration to complete the design of a Glauert-type airfoil. These require that the x/c location corresponding to ϕ_2 and ϕ_4 be at $0.68c$ and $0.62c$, respectively. Table 2 lists the values of some of the design variables after the final converged solution and the respective lift and drag coefficients for each of the design conditions.

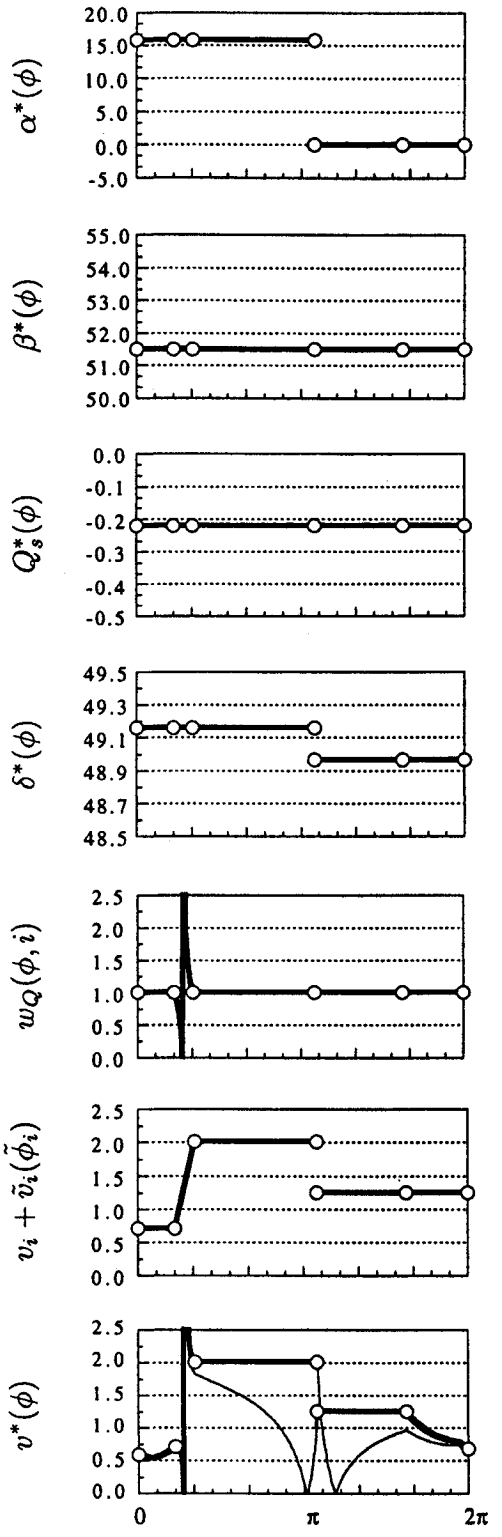

Fig. 7 Distribution of design variables for a five-segment airfoil. The values of $\alpha^*(\phi)$, $\beta^*(\phi)$, and $\delta^*(\phi)$ are in degrees.

Figure 7 shows the final design distributions of $\alpha^*(\phi)$, $\beta^*(\phi)$, $Q_s^*(\phi)$, $\delta^*(\phi)$, $w_Q(\phi, i)$, $v_i + \tilde{v}_i(\tilde{\phi}_i)$, and $v^*(\phi)$, from top-to-bottom, respectively, as a function of the angle ϕ. In Fig. 7, the junction between any two segments is shown by a white circle to indicate the values of the design variables for each of the segments. Although the multipoint design capability of the method allows for the specification of different values for the design variables for different segments based on the design requirements, the previous example does not fully

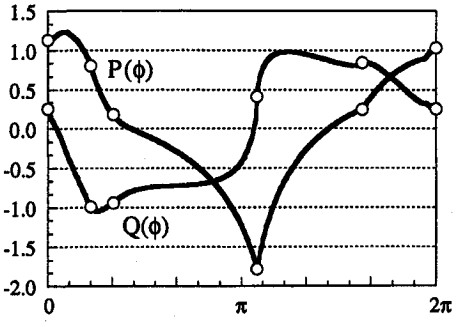

Fig. 8 Harmonic functions $P(\phi)$ and $Q(\phi)$.

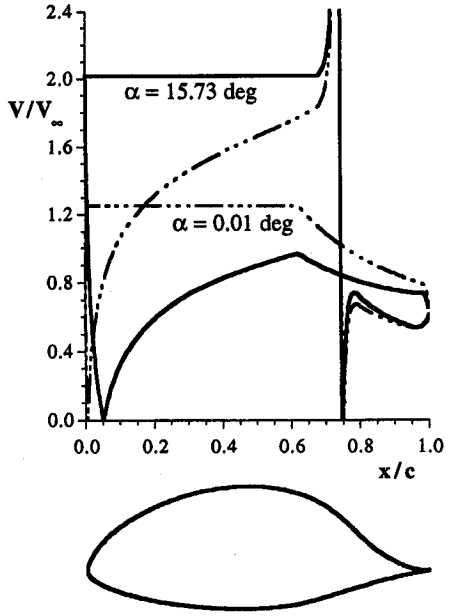

Fig. 9 Airfoil and velocity distribution at $\alpha = 15.73$ and 0.01 deg.

exploit this capability for the sake of simplicity. In the previous example, $\beta^*(\phi)$ and $Q_s^*(\phi)$ were specified as constants, whereas $\alpha^*(\phi)$ was specified as one value for the first three segments and as another value for the last two segments. In addition to it, a linear relative design velocity distribution $\tilde{v}_i(\tilde{\phi}_i)$ was also specified for segment 2.

After the specification of these design variables, $\delta^*(\phi)$ is determined numerically from Eq. (3), $w_Q(\phi, i)$ is determined with the help of Eq. (31), and the velocity levels v_i are obtained from the continuity equation, i.e., Eq. (15). The velocity distributions are then drawn with the help of Eq. (30) at the design $\alpha^*(\phi)$. The thick lines indicate the complete design velocity distribution $v^*(\phi)$ that is used to form $P(\phi)$ along with the other design variables. Then $Q(\phi)$ is determined from the Poisson's integral formula, and finally, both $P(\phi)$ and $Q(\phi)$ are used to obtain the airfoil shape. The harmonic functions $P(\phi)$ and $Q(\phi)$ are shown in Fig. 8 and the resulting airfoil shape is shown in Fig. 9 along with the velocity distributions at $\alpha =$ 15.73 and 0.01 deg.

As a second example, a 13-segment high-lift suction airfoil was designed such that $\beta^*(\phi) = 45.5$ deg, $Q_s^*(\phi) = -0.12$, $K_H = 0.45$, $\bar{K}_H = -0.40$, and $(t/c)_{max} = 0.12$. The resulting airfoil shape and velocity distributions are shown in Fig. 10. It has a C_l of 3.2 and a C_d of 0.0683 at $\alpha = 25$ deg. This example illustrates that quite high lift coefficients can be achieved by employing suction on the airfoil.

Two important observations can be gleaned from example airfoils presented. First, a comparison of the Glauert-like airfoil shown in Fig. 9 with the GLAS II airfoil shown in Fig. 2 indicates that the Glauert airfoil was designed by specifying a

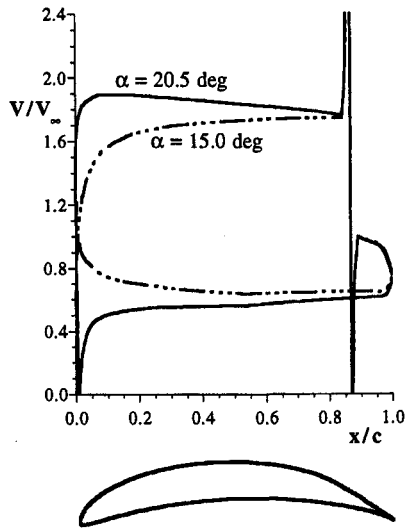

Fig. 10 High-lift suction airfoil and the velocity distributions for α = 20.5 and 15 deg.

step drop in the velocity distribution rather than by actually employing suction at the slot location. The introduction of the step drop in the velocity results in a spiral at the slot location, which interestingly is absent if the effects of suction are included in the specification of the velocity distribution as evident from Fig. 9. Second, both examples confirm that a significant amount of pressure recovery can be achieved by employing suction in the vicinity of the trailing edge.

Conclusions and Recommendations

Several important conclusions can be drawn from this study.

1) It is evident that a discontinuous change in the velocity distribution is not a satisfactory model to represent the behavior of flow in the vicinity of the suction slot, and as a result, it leads to a surface discontinuity in the form of a spiral at the slot location.

2) To accurately model the flow near a suction slot, the velocity must undergo a sink effect, i.e., it must increase in front of the slot and decrease behind it. A good representation of the sink effect can be achieved through the use of a sink at the slot location.

3) A new and versatile method for the multipoint design of suction airfoils in incompressible flow is now available.

4) The method readily generalizes to multiple suction slots.

5) The theory predicts an increased lift coefficient and a nonzero value for the inviscid drag coefficient as a result of employing slot suction on airfoils. The increase in lift coefficient is as a result of an offset provided by suction since the lift–curve slope remains unchanged by suction. Most important of all, the theory predicts that the value of the inviscid drag coefficient is exactly equal to twice the magnitude of the suction coefficient.

6) As evident from the design examples, a significant amount of pressure recovery can be achieved by employing suction.

The fact that a significant amount of pressure recovery can be achieved by employing suction alone is useful in many of the applications related to the advanced-concept wings. For example, suction could be employed over very thick wings to prevent separation of the boundary-layer, which would otherwise result in a huge drag penalty. As another example, thin airfoils could be made to operate at very high angles of attack without flow separation. A natural extension of the present method is, therefore, the integration of the viscous boundary-layer analysis into the design of suction airfoils to enhance its versatility. Lastly, the increased airfoil performance is not without a cost and opens a door to a range of issues that must be addressed and explored to recognize the true merits of slot-suction airfoils.

Acknowledgments

This work was supported under the Advanced Concepts for Aeronautics sponsored by NASA, Office of Aeronautics, Washington, DC. Helpful discussions with John Sullivan of Purdue University and Mark Drela of the Massachusetts Institute of Technology are gratefully acknowledged.

References

[1]Goldschmied, F. R., "Thick-Wing Spanloader All-Freighter: A Design Concept for Tomorrow's Air Cargo," AIAA Paper 90-3198, Sept. 1990.

[2]Glauert, M. B., "The Design of Suction Aerofoils with a Very Large C_L Range," Aeronautical Research Council, R&M 2111, Nov. 1945.

[3]Glauert, M. B., Walker, W. S., Raymer, W. G., and Gregory, N., "Wind Tunnel Tests on a Thick Suction Airfoil with a Single Slot," Aeronautical Research Council, R&M 2646, Oct. 1948.

[4]Glauert, M. B., "The Application of the Exact Method of Aerofoil Design," Aeronautical Research Council, R&M 2683, Oct. 1947.

[5]Dirlik, S., Kimmel, K., Sekelsky, A., and Slomski, J., "Experimental Evaluation of a 50-Percent Thick Airfoil with Blowing and Suction Boundary Layer Control," AIAA Paper 92-4500, Aug. 1992.

[6]Heugen, D. M., "An Experimental Study of a Symmetrical Aerofoil with a Rear Suction Slot, and a Retractable Flap," *Journal of the Royal Aeronautical Society*, Vol. 57, 1953, pp. 627–645.

[7]Howe, H. J., and Neumann, B. J., "An Experimental Evaluation of a Low Propulsive Power, Discrete Suction Concept Applied to an Axisymmetric Vehicle," David W. Taylor Naval Ship R&D Center, TM 16-82/02, 1982.

[8]Preston, J. H., Gregory, N., and Rawcliffe, A. G., "The Theoretical Estimation of Power Requirements for Slot-Suction Aerofoils with Numerical Results for Two Thick Griffith Type Sections," Aeronautical Research Council, R&M 1577, June 1948.

[9]Richards, E. J., and Burge, C. H., "An Airfoil Designed to Give Laminar Flow over the Whole Surface with Boundary-Layer Suction," Aeronautical Research Council, R&M 2263, June 1943.

[10]Richards, E. J., Waler, W. S., and Taylor, C. R., "Wind-Tunnel Tests on 30% Suction Wing," Aeronautical Research Council, R&M 2149, July 1945.

[11]Callaghan, J. T., and Liebeck, R. H., "Some Thoughts on the Design of Subsonic Transport Aircraft for the 21st Century," Douglas Aircraft Co., Paper 901987, Long Beach, CA.

[12]Chaplin, H. R., "Application of Very Thick BLC Airfoils to a Flying Wing Type Transport Aircraft," Society of Automotive Engineers Technical Paper Series 901992, Oct. 1990.

[13]McMasters, J. H., and Kroo, I. M., "Advanced Configurations for Very Large Subsonic Transport Airplanes," NASA Workshop on Potential Impacts of Advanced Aerodynamic Technology on Air System Productivity, NASA–LaRC, 1993.

[14]Lighthill, M. J., "A New Method of Two-Dimensional Aerodynamic Design," Aeronautical Research Council, R&M 2112, April 1945.

[15]Eppler, R., "Direct Calculation of Airfoils from Pressure Distribution," NASA TT F-15, 417, March 1974; translated from *Ingenieur-Archive*, Vol. 25, No. 1, 1957, pp. 32–57.

[16]Eppler, R., *Airfoil Design and Data*, Springer–Verlag, New York, 1990.

[17]Selig, M. S., and Maughmer, M. D., "A Multipoint Inverse Airfoil Design Method Based on Conformal Mapping," *AIAA Journal*, Vol. 30, No. 5, 1992, pp. 1162–1170.

[18]Thwaites, B. (ed.), *Incompressible Aerodynamics*, Dover, New York, 1987, pp. 239–249.

[19]Milne-Thomson, L. M., *Theoretical Aerodynamics*, Dover, New York, 1958, pp. 84, 85.

[20]Glauert, M. B., Walker, W. S., Raymer, W. G., and Gregory, N., "Wind-Tunnel Tests on a Thick Suction Airfoil with a Single Slot," Aeronautical Research Council, R&M 2646, Oct. 1948.